Available online at www.sciencedirect.com
SCIENCE DIRECT®
International Journal of Heat and Mass Transfer 47 (2004) 4849–4855
International Journal of HEAT and MASS TRANSFER
www.elsevier.com/locate/ijhmt

Double porous media model for mass transfer of hemodialyzers

Weiping Ding [a], Liqun He [a,*], Gang Zhao [a], Haifeng Zhang [a], Zhiquan Shu [a], Dayong Gao [a,b]

[a] Department of Thermal Science and Energy Engineering, University of Science and Technology of China, Hefei 230027, PR China

[b] Department of Mechanical Engineering, University of Kentucky, Lexington, KY 40506-0108, USA

Received 25 August 2003; received in revised form 30 April 2004

Abstract

Double porous media model for mass transfer of hollow fiber hemodialyzers is presented. In the model, the hollow fiber bundle is treated as a porous region composed of two interpenetrating porous regions i.e. the blood and dialysate flow regions, and the interface of the two regions is the porous membrane through which mass transfer is performed. Navier–Stokes equations with Darcy source terms are used to describe the flows within the two regions. Modified Kedem–Katchalsky equations as other source terms are added into conservation equations to simulate the permeating flux through the porous membrane. The model is validated with respect to the experimental data in the literature.

1. Introduction

Hemodialyzers have been applied to hemodialysis widely. Common modules consist of bundled hair-like hollow fibers that are potted at two ends and inserted into a cylindrical vessel (Fig. 1). In operation, blood is pumped through the blood inlet, distributed into hollow fibers where excess water and waste products are removed across the membrane due to pressure and concentration differences, and goes out at the blood outlet. At the same time, dialysate is pumped through the dialysate inlet, counter-currently passes between hollow fibers with waste products from the blood, and goes out at the dialysate outlet.

Over the past decades many mass transfer models have been developed to study mass transfer performance and clearance of hemodialyzers. Mass transfer in hemodialyzers involves a combination of convection and diffusion [1]. One might attempt to accurately simulate flow distribution and mass transfer around each hollow fiber with conservation equations. However, this approach would require the discretization of complex regions and the formulation of a large set of equations whose solution would require tremendous computational resources. So, in the literature, most models were one-dimensional, and based upon the assumption that the flow associated with each fiber is identical, so that a single fiber along with the fluid annulus surrounding it is representative of the whole bundle [1–8]. In their models, the radial and circumferential gradients of the blood and dialysate sides (or the lumen and shell sides) were usually neglected. In fact, the flow fields vary not only in the axial direction but also in the radial and circumferential directions because of the inlet and outlet effects [9–12]. Jaffrin [13] reviewed various mass transfer models, and he confessed that the accuracy of one-dimensional models is limited, the rigorous overall mass transfer calculation can not been achieved by these models, and they are only suitable for the middle portion and almost helpless for designers to optimize the inlet and outlet configuration of hemodialyzers.

* Corresponding author. Tel.: +86-551-360-7146; fax: +86-551-360-7346.
E-mail address: heliqun@ustc.edu.cn (L. He).

0017-9310/$ - see front matter © 2004 Elsevier Ltd. All rights reserved.
doi:10.1016/j.ijheatmasstransfer.2004.04.017

Nomenclature

C	solute concentration, kg/m^3
C_{bi}	solute concentration at blood inlet, kg/m^3
C_{bo}	solute concentration at blood outlet, kg/m^3
C_m	solute mean concentration in the membrane, kg/m^3
CL	solute clearance, ml/min
D	solute-free diffusion coefficient, m^2/s
$\boldsymbol{I}$	unit tensor
J_S	solute flow rate across unit membrane area, kg/(m^2 s)
J_V	volumetric flow rate across unit membrane area, m^3/(m^2 s)
k	Darcy permeability, m^2
K_O	overall mass transfer coefficient, m/s
L	effective length of the module, m
L_{wet}	permeable length of the wet fiber, m
L_P	membrane permeability, m/(Pa s)
N	number of hollow fibers
P	hydrostatic pressure, Pa
Q_{bi}	blood flow rate at blood inlet, ml/min
Q_{bo}	blood flow rate at blood outlet, ml/min
Q_{di}	dialysate flow rate at dialysate inlet, ml/min
Q_f	total ultrafiltration rate, ml/min
R	universal gas constant, J/(mol K)
R_M	module inner radius, m
R_O	fiber outer radius, m
R_I	fiber inner radius, m
S_1	mass source/sink term
S_2	solute source/sink term
T	absolute temperature, K
$\boldsymbol{u}$	actual fluid velocity vector, m/s

Greek symbols

β	membrane area per unit volume, m^2/m^3
ε	porosity
μ	fluid viscosity, N s/m^2
ρ	fluid density, kg/m^3
σ	solute reflection coefficient
ϕ	fraction of the volume occupied by the fibers

Subscripts and superscripts

b	blood
d	dialysate
i	z-, r-, or θ-direction
T	transpose of a matrix

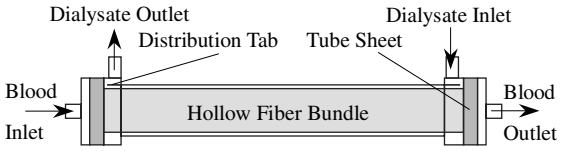

Fig. 1. Typical hollow fiber hemodialyzer module.

So, to deal with the overall mass transfer performance and optimize the current hemodialyzers especially including the inlet and outlet configuration, the more effective mass transfer model need to be developed. For dialyzer modules containing thousands of hollow fibers, porous media model based on *volume averaged* technique, can describe transport phenomena within the modules effectively [11,14,15]. In the literature the shell side was usually treated as porous media region, while the lumen side seldom [16–19]. Labecki et al. [20] and Lemanski and Lipscomb [11] treated the lumen side as porous media region to predict the redistribution of protein in the shell side and the production of nitrogen from air, respectively. But their models cannot be used to investigate the complex overall mass transfer of hemodialyzers directly.

In this article, a more effective model for mass transfer of hemodialyzers is attempted to develop, which can be used to study the overall mass transfer performance, investigate the effects of the inlet and outlet configuration, and optimize the design of hemodialyzers.

2. Theory modeling

In the process of hemodialysis, blood and dialysate all pass two regions i.e. inlet and outlet region and hollow fiber bundle region. Obviously the flow in the inlet and outlet region can be described by Navier–Stokes equation, while the other can be described by Darcy equation. In order to avoid complex boundary conditions between the two regions, Navier–Stokes equation with Darcy term is used to simulate the flow in the hollow fiber bundle region. So conservation equations of the two regions can be described in the same form.

In this paper, the blood and dialysate sides of hollow fiber bundle are modeled as two interpenetrating porous regions, and the interface of the two regions is the porous membrane. This model presents a new idea i.e. double porous media idea or interdependent porous media idea.

Under the following assumptions the model is developed: (a) Properties of all fibers are equal and

constant; (b) The distribution of fibers is uniform; (c) The hollow fiber bundle is axisymmetric and anisotropic; (d) Flows are isothermal, steady-state, laminar; (e) Hydrostatic forces are negligible; (f) Kinetics of solute adsorption is negligible; (g) The effect of mass exchange upon momentum is negligible; (h) The expansion of fibers under wet conditions is neglected.

2.1. Dialysate (shell) flow

The dialysate flow can be described by the following equations:

Continuity equation:

$$\nabla \cdot (\rho_{\mathrm{d}} \boldsymbol{u}_{\mathrm{d}}) = S_1/\varepsilon_{\mathrm{d}} \tag{1a}$$

Momentum equation:

$$\nabla \cdot (\rho_{\mathrm{d}} \boldsymbol{u}_{\mathrm{d}} \boldsymbol{u}_{\mathrm{d}}) = -\nabla P_{\mathrm{d}} + \nabla \cdot \left[\mu_{\mathrm{d}} (\nabla \boldsymbol{u}_{\mathrm{d}} + \nabla \boldsymbol{u}_{\mathrm{d}}^{\mathrm{T}}) - \frac{2}{3} \mu_{\mathrm{d}} (\nabla \cdot \boldsymbol{u}_{\mathrm{d}}) \boldsymbol{I} \right] - \frac{\mu_{\mathrm{d}}}{k_{i,\mathrm{d}}} \boldsymbol{u}_{\mathrm{d}} \tag{1b}$$

Concentration equation:

$$\nabla \cdot (\rho_{\mathrm{d}} \boldsymbol{u}_{\mathrm{d}} C_{\mathrm{d}}) = \nabla \cdot (\rho_{\mathrm{d}} D_{i,\mathrm{d}} \nabla C_{\mathrm{d}}) + S_2/\varepsilon_{\mathrm{d}} \tag{1c}$$

2.2. Blood (Lumen) flow

The blood flow can be described by the following equations:

Continuity equation:

$$\nabla \cdot (\rho_{\mathrm{b}} \boldsymbol{u}_{\mathrm{b}}) = -S_1/\varepsilon_{\mathrm{b}} \tag{2a}$$

Momentum equation:

$$\nabla \cdot (\rho_{\mathrm{b}} \boldsymbol{u}_{\mathrm{b}} \boldsymbol{u}_{\mathrm{b}}) = -\nabla P_{\mathrm{b}} + \nabla \cdot \left[\mu_{\mathrm{b}} (\nabla \boldsymbol{u}_{\mathrm{b}} + \nabla \boldsymbol{u}_{\mathrm{b}}^{\mathrm{T}}) - \frac{2}{3} \mu_{\mathrm{b}} (\nabla \cdot \boldsymbol{u}_{\mathrm{b}}) \boldsymbol{I} \right] - \frac{\mu_{\mathrm{b}}}{k_{i,\mathrm{b}}} \boldsymbol{u}_{\mathrm{b}} \tag{2b}$$

Concentration equation:

$$\nabla \cdot (\rho_{\mathrm{b}} \boldsymbol{u}_{\mathrm{b}} C_{\mathrm{b}}) = \nabla \cdot (\rho_{\mathrm{b}} D_{i,\mathrm{b}} \nabla C_{\mathrm{b}}) - S_2/\varepsilon_{\mathrm{b}} \tag{2c}$$

2.3. Transmembrane flow

Kedem and Katchalsky [21] developed famous K–K equations to describe mass transfer across the porous membrane. But their equations cannot be used directly because mass transport resistances in both shell and lumen sides cannot be neglected. So in the modified K–K equations, the solute permeability is substituted with the overall mass transfer coefficient [1].

$$J_{\mathrm{V}} = L_P[(P_{\mathrm{b}} - P_{\mathrm{d}}) - \sigma RT \cdot (C_{\mathrm{b}} - C_{\mathrm{d}})] \tag{3}$$

$$J_{\mathrm{S}} = (1 - \sigma) C_{\mathrm{m}} J_{\mathrm{V}} + K_{\mathrm{O}} \cdot (C_{\mathrm{b}} - C_{\mathrm{d}}) \tag{4}$$

2.4. Source/sink terms

In Eqs. (1) and (2), S_1 is the mass source/sink term which is due to fluid leakage across the membrane, and S_2 is the solute source/sink term which is due to solute leakage across the membrane. Source/sink terms can be determined by using the following relations:

$$S_1 = J_{\mathrm{V}} \cdot \beta \cdot \rho_{\mathrm{b}} \quad (J_{\mathrm{V}} \geqslant 0) \tag{5a}$$

$$S_1 = J_{\mathrm{V}} \cdot \beta \cdot \rho_{\mathrm{d}} \quad (J_{\mathrm{V}} < 0) \tag{5b}$$

$$S_2 = J_{\mathrm{S}} \cdot \beta \cdot \rho_{\mathrm{b}} \quad (J_{\mathrm{S}} \geqslant 0) \tag{6a}$$

$$S_2 = J_{\mathrm{S}} \cdot \beta \cdot \rho_{\mathrm{d}} \quad (J_{\mathrm{S}} < 0) \tag{6b}$$

$$\beta = \frac{N \cdot 2\pi R_I L_{\mathrm{wet}}}{\pi R_{\mathrm{M}}^2 L} \tag{7}$$

2.5. Clearance calculation

Generally, the following equation is used to calculate the solute clearance:

$$CL = (Q_{\mathrm{bi}} C_{\mathrm{bi}} - Q_{\mathrm{bo}} C_{\mathrm{bo}})/C_{\mathrm{bi}} \tag{8}$$

3. Simulation condition

3.1. Boundary condition

According to the literature [9,22], blood flow can be simplified as a two-dimensional flow with axial and radial components. Dialysate flow is more complex, but it can still be approximated as a two-dimensional flow to some extent because of the special design of distribution tabs at the dialysate inlet and outlet. The spatial domain of the hollow fiber bundle under consideration is depicted in Fig. 2. The boundary conditions are shown in Table 1.

3.2. Parameter estimation

Geometric parameters of the modules and transport parameters of membranes are shown in Table 2 and Table 3, respectively.

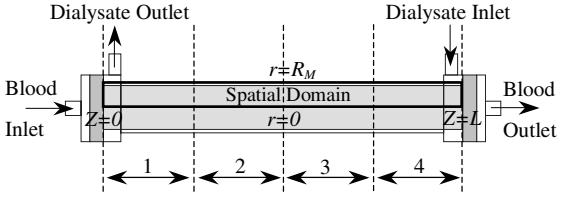

Fig. 2. Diagram of the spatial domain boundaries.

Table 1
Boundary conditions

Region	z	r	Condition
Blood (lumen)	Any	0	$\partial P_b/\partial r = 0$, $\partial C_b/\partial r = 0$
	Any	R_M	$\partial P_b/\partial r = 0$, $\partial C_b/\partial r = 0$
	0	Any	$\partial P_b/\partial z = -\mu \cdot \boldsymbol{u}_b(r)/k_{z,b}$, $C_b(r) = C_{bin}$
	L	Any	$P_b = P_b(r)$, $\partial C_b/\partial z = 0$
Dialysate (shell)	Any	0	$\partial P_d/\partial r = 0$, $\partial C_d/\partial r = 0$
	Any	R_M	$\partial P_d/\partial r = 0$, $\partial C_d/\partial r = 0$
	0	Any	$\partial P_d/\partial z = -\mu \cdot \boldsymbol{u}_d(r)/k_{z,d}$, $C_d(r) = C_{din}$
	L	Any	$P_d = P_d(r)$, $\partial C_d/\partial z = 0$

Table 2
Geometric characteristics[a] of the hollow fiber modules used for clearance predictions

Module type	Membrane material	Effective length (cm)	Membrane area (m^2)	Fiber inner diameter (μm)	Fiber outer diameter (μm)	Module diameter (cm)
CT190G	Cellulose triacetate	24	1.90	200	230	3.5
Syntra160	Polyethersulfone	22	1.60	200	260	3.9
Hospal Filtral 12	AN 69 HF	20	1.15	220	310	3.9

[a] Data from the manufacturer.

Table 3
Transport and separation characteristics* of the membrane used for clearance predictions

Module type	L_P m/(Pa s) (water)	Urea (60 Dalton) σ/K_O (m/s)	Creatinine (113 Dalton) σ/K_O (m/s)	Vitamin B_{12} (1355 Dalton) σ/K_O (m/s)
CT190G	1.15e-10**	0.0/1.082e-05	0.0/7.219e-06	–/–
Syntra160	5.55e-10***	–/–	–/–	–/–
Hospal Filtral 12	5.63e-11	–/–	0.0/4.172e-06****	0.0/1.675e-06****

*Data from the manufacturer except for:
**By Liao [19];
***By Peter et al. [26];
****By fitting model predicted clearances to experimental ones [1].

According to the literature [1,8,19], saline solution and water were substituted for blood and dialysate, respectively. The solution properties adopted water properties at 310.15K. The free diffusion coefficient of urea was 1.82×10^{-9} m^2/s, and creatinine was 1.29×10^{-9} m^2/s [23].

Darcy permeability k is a function of the bundle geometry [14] and D is typically composed of contributions from molecular diffusion and Taylor dispersion [24]. In this paper, the following equations were adopted to estimate their values [15,20].

$$k_{z,b} = \frac{nR_I^4 L}{8R_M^2 L_{wet}\varepsilon_b} \tag{9a}$$

$$k_{z,d} = \frac{R_O^2 L^2}{4\phi L_{wet}^2 \varepsilon_d}\left(-\ln\phi - \frac{3}{2} + 2\phi - \frac{1}{2}\phi^2\right) \tag{9b}$$

$$k_{r,d} = \frac{R_O^2}{8\phi\varepsilon_d}\left(-\ln\phi + \frac{\phi^2-1}{\phi^2+1}\right) \tag{9c}$$

$$D_{r,d} = \frac{D}{2-\varepsilon_d} \tag{10a}$$

$$D_{z,d} = \frac{DL^2}{L_{wet}^2} \tag{10b}$$

where, the porosity of the dialysate side $\varepsilon_d = 1 - nR_O^2 L_{wet}/(R_M^2 L)$, the porosity of the blood side $\varepsilon_b = nR_I^2 L_{wet}/(R_M^2 L)$, and the fraction of the volume occupied by the fibers $\phi = 1 - \varepsilon_d$. $D_{z,b}$ was assumed to be $D(L/L_{wet})^2$. Since the fibers are not directly connected with one another, the Darcy permeability and diffusion coefficient of blood side in radial direction can be set to zero.

3.3. Numerical method

The boundary conditions adopted the even flow rate and solute concentration at the inlet of blood and dialysate, and the pressure at the outlet of blood and dialy-

sate. The outlet pressure of dialysate was set to 0, and the outlet pressure of blood was adjusted according to the total ultrafiltration rate $Q_f = Q_{bi} - Q_{bo}$. The finite difference method was used to discretize the above equations, and SIMPLER algorithm was used to calculate flow fields [25]. A 61×61 grid was chosen for all simulations based on a mesh-refinement analysis. Increasing the grid from 61×61 to 81×81 gave values that differed by less than 0.5% over the entire region considered.

4. Result and discussion (validation of the model)

4.1. Model predictions for solute clearance

Model predictions for solute clearance were validated with respect to the experimental data by Liao [19] with a CT190G module using saline solution in substitution of the blood. Two solutes were used: Urea (60 Dalton) and Creatinine (113 Dalton).

Reliable values of the overall mass transfer coefficient K_O were not found in the literature. So, K_O was estimated for each solute by using the following method [1]. Firstly, one case with experimental results is chosen as standard case. Then the case is used to fit numerical results with experimental results to get K_O. Finally, K_O is used to predict other cases.

In this paper, the case ($Q_{bi} = Q_{di} = 400$ ml/min) is used as standard case. The fitted K_O is shown in Table 3. The predicted results are shown in Table 4.

The results show that the numerical results are in good agreement with experimental results. When blood flow rate is fixed, clearance increases with increasing dialysate flow rate. But in some cases, the error is higher than 5%. The reasons which cause the error maybe are: (1) In the simulation, in order to simplify the calculation, we only took two-dimensional situation into account, and ignored the inlet and outlet effect of the module. In fact the inlet and outlet effect affects mass transfer greatly [9,12]. The effect is different with different velocities of blood and dialysate inflow. But if we take into the inlet and outlet effect account, we have to deal with three-dimensional numerical simulation. This will be discussed in another paper in detail. (2) The assumption of uniform packed hollow fibers is not very accurate, and the overall mass transfer coefficient is not constant. (3) Probably, some errors exist in the experimental data.

4.2. Model predictions for ultrafiltration rate

Model predictions for ultrafiltration rate were validated with respect to the experimental work by Peter et al. [26] with a SYNTRA160 module using water in substitution of the blood and dialysate. In the experiment, the flow was channeled into the blood side and recirculated in a counter-current fashion through the dialysate side. The magnetic resonance Fourier velocity imaging technique was used to measure the velocity at each location (Fig. 2). Two flow rates were used: 300 and 600 ml/min. Then the ultrafiltration rate between the two closer locations was estimate. So in our calculation, the outlet pressure of blood was set to be higher than the inlet pressure of dialysate and was acquired by fitting the numerical result with the experimental result at Section 3.

Fig. 3 shows that the predicted ultrafiltration rates agree with the experimental results. The ultrafiltration

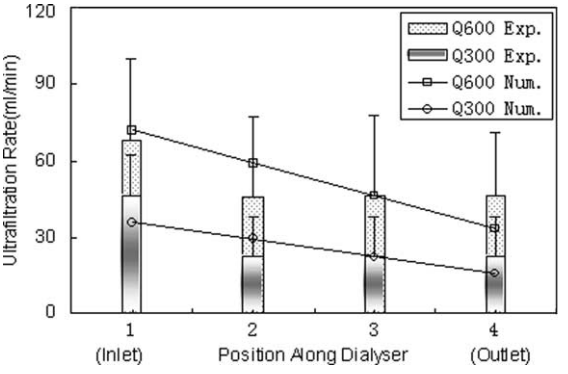

Fig. 3. Comparison of theoretical and experimental ultrafiltration rate.

Table 4
Comparison of experimental and theoretical clearance with CT190G module [19]

Q_{bi} (ml/min)	Q_{di} (ml/min)	Urea			Creatinine		
		Exp.	Num.	Error (%)	Exp.	Num.	Error (%)
300	200	195.56	188.18	3.77	185.98	177.29	4.67
300	300	234.83	235.21	0.16	215.82	214.46	0.63
300	400	266.56	256.82	3.65	248.12	232.76	6.19
400	200	212.34	196.45	7.48	207.31	187.11	9.74
400	400	294.49	294.57	0.03	262.58	262.62	0.02
400	500	305.62	315.50	3.23	274.14	279.13	1.82

rate decreases along the length of the SYNTRA160 module. But at the inlet and outlet, the predicted values deviate from the experimental results. Although some errors maybe exist in the experiment [26], the fact that the effect of the inlet and outlet configuration was not taken into account in the simulation is a primary reason. However, one should know the fact that although the model of this article solves the formulation of control equations, the three-dimensional discretization of the complex inlet and outlet region is another challenge.

4.3. Effect of total ultrafiltration rate on clearance

Clearance enhancement is generally related to clearance under a null total ultrafiltration rate CL_0, the total ultrafiltration rate Q_f, the overall mass transfer coefficient K_O, and the solute reflection coefficient. The enhancement of creatinine and vitamin B_{12} (1355 Dalton) clearance predicted by our model with increasing total ultrafiltration rate is shown in Tables 5 and 6.

The results show that the model in this paper, as well as other models in the literature, yields clearance enhancements in good agreement with experimental data. Comparing the predictions of the model in this paper with those of other ones in the literature, the model of this article does not indeed indicate its advantage. However, even so, the mentioned models here were all one-dimensional, and could not be extended to discuss the overall mass transfer and optimize the configuration of hemodialyzers, but our model can be extended to do so.

4.4. Average solute concentration along the length

Fig. 4 shows the theoretical cross-sectional average concentration of urea along the length of the CT190G module. The tendency is qualitatively consistent with the experimental cross-sectional average concentration in the literature [9]. The results show that the cross-sectional average urea concentration decreases along the blood flow direction, the average urea concentration in dialysate increases along the dialysate flow direction, and the average urea concentration in blood is always higher than that in dialysate from blood inlet to blood outlet.

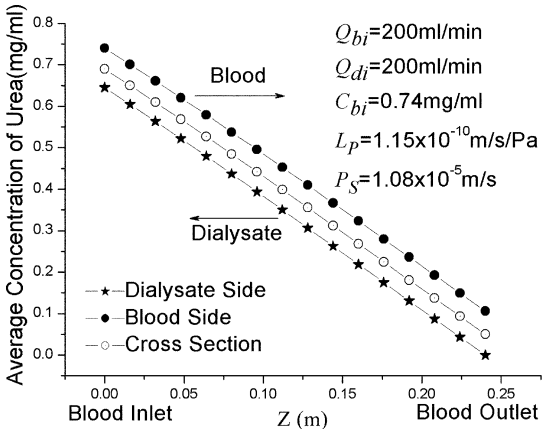

Fig. 4. Variation of urea concentration along the length of the module (blood side, dialysate side, and cross section).

Table 5
Comparison of experimental and theoretical enhancement of creatinine clearance predicted by different models with increasing total ultrafiltration rates

Q_f (ml/min) model	$(CL - CL_0)/CL_0$				
	Experimental [1]	Sargent et al. [27]	Chang et al. [4]	Jaffrin et al. [1]	This paper
20	0.0460	0.0447	0.0695	0.0667	0.0526
40	0.1151	0.0894	0.1390	0.1355	0.1052
60	0.1785	0.1340	0.2084	0.2032	0.1576

Data for a Hospal Filtral 12 module operated with saline solution at $Q_{bi} = 195$ ml/min, $Q_{di} = 500$ ml/min.

Table 6
Comparison of experimental and theoretical enhancement of vitamin B_{12} clearance predicted by different models with increasing total ultrafiltration rates

Q_f (ml/min) model	$(CL - CL_0)/CL_0$				
	Experimental [1]	Sargent et al. [27]	Chang et al. [4]	Jaffrin et al. [1]	This paper
20	0.1155	0.1443	0.1730	0.1161	0.1171
40	0.2135	0.2886	0.3460	0.2322	0.2397
60	0.3893	0.4329	0.5191	0.3483	0.3682

Data for a Hospal Filtral 12 module operated with saline solution at $Q_{bi} = 185$ ml/min, $Q_{di} = 500$ ml/min.

5. Conclusions

1. In this paper double porous media model for mass transfer of hollow fiber hemodialyzers is presented. In the model, a hollow fiber bundle is considered as a porous region which is composed of two interpenetrating porous flow regions. The interface of the two regions is the membrane through which mass transfer is performed. This model embodies a new idea i.e. double porous media idea or interdependent porous media idea.
2. Modified Kedem–Katchalsky equations as source terms, which describe mass transfer between blood and dialysate, are added to conservation equations to simulate the transmembrane flow.
3. Model predictions agree well with the experimental work in the literature, and the model is validated by these experimental data.

Acknowledgements

The help of Prof. Chen Yi-liang is gratefully acknowledged. The work is supported by the Project of Chinese Academy of Sciences on Hundreds of Scholars (2000–2003).

References

[1] M.Y. Jaffrin, L. Ding, J.M. Laurent, Simultaneous convective and diffusive mass transfers in a hemodialyzer, J. Biomech. Eng. 112 (1990) 212–219.
[2] I. Noda, C.C. Gryte, Mass transfer in regular arrays of hollow fibers in countercurrent dialysis, AIChE J. 25 (1979) 113–122.
[3] C. Gostoli, A. Gatta, Mass transfer in a hollow fiber dialyzer, J. Membr. Sci. 6 (1980) 133–148.
[4] Y.L. Chang, C.J. Lee, Solute transport characteristics in hemodiafiltration, J. Membr. Sci. 39 (1988) 99–111.
[5] D.G. Taylor, J.M. Piret, B.D. Bowen, Protein polarization in isotropic membrane hollow-fiber bioreactors, AIChE J. 40 (1994) 321–333.
[6] A. Wüpper, D. Woermann, F. Dellanna, C.A. Baldamus, Retrofilration rates in high-flux fiber hemodialyzers: analysis of clinical data, J. Membr. Sci. 121 (1996) 109–116.
[7] A. Wüpper, F. Dellanna, C.A. Baldamus, D. Woermann, Local transport processes in high-flux hollow fiber dialyzers, J. Membr. Sci. 131 (1997) 181–193.
[8] C. Legallais, G. Catapano, B. Harten, U. Baurmeister, A theoretical model to predict the in vitro performance of hemodialfilters, J. Membr. Sci. 168 (2000) 3–15.
[9] A. Frank, G.G. Lipscomb, M. Dennis, Visualization of concentration fields in hemodialyzers by computed tomography, J. Membr. Sci. 175 (2000) 239–251.
[10] J. Wu, V. Chen, Shell-side mass transfer performance of randomly packed hollow fiber modules, J. Membr. Sci. 172 (2000) 59–74.
[11] J. Lemanski, G.G. Lipscomb, Effect of shell-side flows on the performance of hollow-fiber gas separation modules, J. Membr. Sci. 195 (2001) 215–228.
[12] W. Ding, L. He, G. Zhao, X. Luo, M. Zhou, D. Gao, Effect of distribution tabs on mass transfer of artificial kidney, AIChE J. 50 (2004) 786–790.
[13] M. Jaffrin, Convective mass transfer in hemodialysis, Artif. Organs 19 (1995) 1162–1171.
[14] L. Skartsis, B. Khomami, J. Kardos, Resin flow through fiber beds during composite manufacturing process I: Review of Newtonian flowthrough fiber beds, II: Numerical and experimental studies of Newtonian flow through ideal and actual fiber beds, Polym. Eng. Sci. 32 (1992) 221–239.
[15] M. Labecki, J.M. Piret, B.D. Bowen, Two-dimensional analysis of fluid flow in hollow-fibre modules, Chem. Eng. Sci. 50 (1995) 3369–3384.
[16] J. Lemanski, G.G. Lipscomb, Effect of shell-side flows on hollow-fiber membrane device performance, AIChE J. 41 (1995) 2322–2326.
[17] T. Osuga, T. Obata, H. Ikehira, S. Tanada, Y. Sasaki, H. Naito, Dialysate pressure isobars in a hollow-fiber dialyzer determined from magnetic resonance imaging and numerical simulation of dialysate flow, Artif. Organs 22 (1998) 907–909.
[18] Petr Doleček, Jiří Cakl, Permeate flow in hexagonal 19-channel inorganic membrane under filtration and backflush operating modes, J. Membr. Sci. 149 (1998) 171–179.
[19] Z.J. Liao, Numerical and experimental studies of mass transfer in artificial kidney and hemodialysis, Ph.D. Dissertation, University of Kentucky, USA, 2002.
[20] M. Labecki, B.D. Bowen, J.M. Piret, Two-dimensional analysis of protein transport in the extracapillary space of hollow-fibre bioreactors, Chem. Eng. Sci. 51 (1996) 4197–4213.
[21] O. Kedem, A. Katchalsky, Thermodynamics analysis of the permeability of biological membranes to non-electrolytes, Biochim. Biophys. Acta 27 (1958) 229–246.
[22] J. Zhang, D. Parker, J.K. Leypoldt, Flow distribution in hollow fiber hemodialysis using magnetic resonance Fourier velocity imaging, ASAIO J. 41 (1995) 678–682.
[23] R. Wendt, E. Klein, E. Bresler, F. Holland, R. Serino, H. Villa, Sieving properties in hemodialysis membranes, J. Membr. Sci. 5 (1979) 23–49.
[24] E.L. Cussler, Diffusion: Mass Transfer in Fluid Systems, second ed., Cambridge University Press, Cambridge, 1997.
[25] S.V. Patankar, Numerical Heat Transfer and Fluid Flow, Hemisphere Publishing Co., 1980.
[26] A. Hardy Peter, C.K. Poh, Z.J. Liao, W.R. Clark, D. Gao, The use of magnetic resonance imaging to measure the local ultrafiltration rate in hemodialyzers, J. Membr. Sci. 204 (2002) 195–205.
[27] J.A. Sargent, F.A. Gotch, Principles and biophysics of dialysis, in: W. Drukker, F.M. Parsons, J.F. Maher (Eds.), Replacement of Renal Function by Dialysis, Martinus Nijhoff Medical Division, The Hague, 1978, pp. 38–68.